

Optimal Quantum Estimation with Stabilizer-Based Local Measurements

Jia-Xuan Liu,¹ Hai-Long Shi,² Chunfeng Wu,^{3,*} and Sixia Yu^{1,4,†}

¹Hefei National Research Center for Physical Sciences at the Microscale and School of Physical Sciences,
Department of Modern Physics, University of Science and Technology of China, Hefei, Anhui 230026, China

²QSTAR, INO-CNR, and LENS, Largo Enrico Fermi 2, 50125 Firenze, Italy

³Science, Mathematics and Technology, Singapore University of Technology and Design, 8 Somapah Road, Singapore 487372, Singapore

⁴Hefei National Laboratory, University of Science and Technology of China, Hefei 230088, China

(Dated: August 12, 2025)

A central challenge in quantum metrology is to identify optimal protocols under measurement constraints that reflect realistic experimental conditions, e.g., local measurements in multipartite scenarios. Here, we present a sufficient criterion for metrological schemes to saturate the quantum Cramér-Rao bound (QCRB) using local measurements, based on stabilizer formalism. In ideal settings, we show that graph states always admit local estimation protocols with an optimal estimation precision determined only by the underlying graph structure. A family of graph states is identified as probe states that achieve suboptimal precision scaling. In noisy environments, we construct several subspaces of probe states (mixed in general) that not only saturate the QCRB with local measurements but also maintain approximately invariant precision scaling. These subspaces offer multiple metrological advantages, including high precision, partial noise resilience, and noise-correcting capability prior to parameter encoding. Under dephasing noise, they exhibit markedly better performance than Greenberger-Horne-Zeilinger states. Our results advance the framework for local-measurement quantum metrology, achieving a robust trade-off between precision and noise tolerance.

Introduction.— Identifying resource states and leveraging local measurements to achieve high precision in quantum metrology is a task of fundamental theoretical and practical significance [1–13]. Remarkably, Greenberger-Horne-Zeilinger (GHZ) states [14], as a class of multipartite entangled states, enable the estimation of a parameter θ with a mean squared error (MSE) $(\Delta\Theta)^2 \sim 1/N^2$ through local measurements, achieving the Heisenberg limit (HL) — an $O(N)$ improvement over entanglement-free protocols [15]. However, whether more general resource states with similar error scaling exist and how to design universal local measurement schemes remain largely unexplored.

In practice, the unavoidable presence of environmental noise destroys quantum coherence [16–18], leading to a significant reduction in sensing precision [19–22]. Particularly in the noisy intermediate-scale quantum (NISQ) era [23, 24], strategies such as quantum error correction [25–28], dynamical decoupling [29–31], time optimization [32, 33], and feedback control [34–36] have been proposed to mitigate the effects of noise. Inspired by the development of noisy quantum metrology, two critical questions naturally arise: (i) Can the error achieve the HL under local measurements while remaining robust against a wide range of noise? (ii) Can noise resistance be further enhanced through strategies involving only local operations?

In this letter, we address the above questions comprehensively. We first propose a sufficient criterion for local measurements to achieve the optimal MSE, forming the basis for constructing subsequent schemes. When applied to noiseless environments, we prove that graph states [37] universally satisfy the criterion, and ideal precision can be achieved by tuning the graph structure. When applied to noisy envi-

ronments, we identify multiple subspaces of high-precision resource states that meet the criterion and exhibit noise robustness. These subspaces not only allow flexible selection based on precision-robustness trade-offs but can also further enhance noise resistance through quantum error correction. We find that stabilizers are the core link connecting precision, noise robustness, and error optimality; their efficient utilization is key to constructing optimal local measurement-based quantum metrology schemes. Our results lay the groundwork for identifying characteristic quantum resources in local measurement-based quantum metrology and quantitative understanding of the relationship between precision and noise.

Preliminaries.— A typical quantum metrology protocol involves initializing a probe state ρ_0 , encoding an unknown real parameter θ via a quantum channel \mathcal{E}_θ to obtain ρ_θ , and estimating θ through quantum measurements $\{\Pi_x\}$ [38]. The MSE $(\Delta\Theta)^2$ of an unbiased estimator Θ , will be lower bounded as $(\Delta\Theta)^2 \geq (\mu\mathcal{I})^{-1}$, where \mathcal{I} is the classical Fisher information (CFI) and μ is the number of repetitions of the experiment. This bound can always be attained by appropriately selecting Θ as $\mu \rightarrow \infty$. \mathcal{I} depends on the form of $\{\Pi_x\}$, and its upper bound (known as the quantum Cramér-Rao Bound [39, 40], QCRB), the quantum Fisher information (QFI) $\mathcal{F} = \text{Tr}(\rho_\theta L_\theta^2)$, can always be realized through projective measurements of the eigenstates of the symmetric logarithmic derivative operator L_θ , defined by $\frac{\partial \rho_\theta}{\partial \theta} = \frac{1}{2}(\rho_\theta L_\theta + L_\theta \rho_\theta)$ [40]. Considering limited experimental resources [41], it is desirable to have an optimal local measurement $\Pi_x = \otimes_{i=1}^N \pi_{x_i}^{(i)}$, where $\sum_{x_i} \pi_{x_i}^{(i)} = I_i$ [7, 42], whose capability is limited. We refer to these protocols as local protocols. As not all parameterized states can saturate the QCRB through local measurements [42], a key problem in measurement-constrained quantum metrology is to identify as many local protocols as possible. To address this, we focus on unitary phase estimation models. We propose a method leveraging stabilizers to recognize local protocols, which is broadly applicable to arbitrary numbers of qubit and

* chunfeng_wu@sutd.edu.sg

† yusixia@ustc.edu.cn

parameter values, in comparison with Ref. [12].

Sufficient Condition for Local Protocols.— We introduce our sufficient condition for identifying local protocols through stabilizers.

Theorem *In a phase estimation model $\rho_\theta = e^{-i\frac{\theta}{2}H} \rho e^{i\frac{\theta}{2}H}$ for N -qubit, where $H = \sum_j H_j$ with H_j acting only on the j -th qubit, if there exist a collective observable K and N single-qubit observables $\{\Omega_k\}_{k \in V}$ such that*

- (i) K stabilizes all states in the support of ρ ;
- (ii) $\{\Omega_k, H_k\} = 0$ ($k \in V$);
- (iii) $[\Omega_k, K] = 0$ ($k \in V$);
- (iv) $\{K, H_k\} = 0$ ($k \in V$).

Then, regardless of the value of θ , the QCRB can be saturated by local measurements.

If the conditions of the aforementioned theorem are satisfied, the admissible local measurement is expressed as $\Omega_V(\theta) = e^{-i\frac{\theta}{2}H} \left(\prod_{i \in V} \Omega_i \right) e^{i\frac{\theta}{2}H}$. The sufficient condition above points out a straightforward way of designing local protocols: we start with a stabilizer of the probe state and construct local Hamiltonian and measurements using the commutations relations as required in the Theorem. This is extremely effective when the stabilizer K is a direct product of traceless local operators, i.e., $K = \prod_i K_i$ with K_i acting only on the i -th qubit and $\text{Tr} K_i = 0$. In fact we have only to choose local measurements to be $\Omega_i = K_i$ and the local Hamiltonian H_i to be orthogonal to K_i so that all the conditions in the Theorem are met.

Corollary *Given a probe state ρ , corresponding to any local stabilizer $K = \prod_i K_i$ with $\text{Tr} K_i = 0$ there is a unitary phase estimation model with optimal local measurements.*

As an immediate application, we take the probe state to be the GHZ state $\rho = |\text{GHZ}_N\rangle\langle\text{GHZ}_N|$ where $|\text{GHZ}_N\rangle \equiv \frac{1}{\sqrt{2}}(|+\rangle^{\otimes N} + |-\rangle^{\otimes N})$. Starting from its stabilizer $Z_V = \prod_{i=1}^N Z_i$, we choose local Hamiltonian to be $H = \sum_{i=1}^N X_i$ and local measurement to be $\Omega_i = Z_i$ we arrive at the standard local protocol using GHZ state. Based on this observation and the stabilizer structure of graph states, we can identify local protocols with high-rate precision and also working efficiently under noisy environments.

Local estimation protocol via graph State.— Given a connected undirected graph $G(V, E)$, with vertex set V and edge set E , we denote by \mathcal{A}_i the neighborhood of the vertex i , the subset of vertices connected to i . Vertices having a single neighbor, i.e., satisfying $|\mathcal{A}_i| = 1$, is called a leaf vertex, and the unique vertex j adjacent to leaf vertex i is referred to as its root vertex and by R, L we denote the sets of all root and leaf vertices, respectively. A pair of vertices j and k is called twins or true twins if and only if $\mathcal{A}_j = \mathcal{A}_k$ or $\mathcal{A}_j + \{j\} = \mathcal{A}_k + \{k\}$ as illustrated in Figs. 1(a) and 1(b), respectively. As the relation of being twins or true twins is an equivalence relation, all the vertices can be partitioned accordingly into two collections of disjoint subsets $\{\mathcal{V}_1, \mathcal{V}_2, \dots, \mathcal{V}_m, \dots\}$ and $\{\mathcal{U}_1, \mathcal{U}_2, \dots, \mathcal{U}_n, \dots\}$, in which all vertices in \mathcal{V}_m (\mathcal{U}_n) are mutually twins (true twins). For later use we denote by $U = \cup_{|\mathcal{U}_n|=1} \mathcal{U}_n$ the set of all vertices that are not true twins

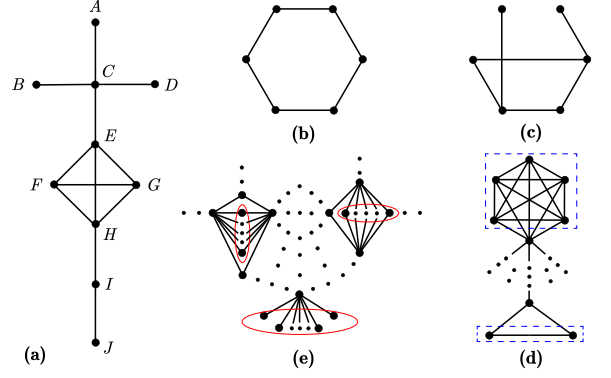


FIG. 1. Graph state structures. (a) The ten-qubit graph contains the twins equivalence class $\{A, B, D\}$ with $\mathcal{A}_A = \mathcal{A}_B = \mathcal{A}_D = \{C\}$, the true twins equivalence class $\{F, G\}$ with $\mathcal{A}_F + \{F\} = \mathcal{A}_G + \{G\} = \{E, F, G, H\}$, and leaf vertices $\{A, B, D, J\}$ with $|\mathcal{A}_A| = |\mathcal{A}_B| = |\mathcal{A}_D| = |\mathcal{A}_J| = 1$. (b) The six-qubit graph state does not contain the above geometric structures. (c) The six-qubit graph state has $\max_\alpha \mathcal{F}_\alpha(G) = 10 < \mathcal{F}(G) = 12$, unable to achieve Eq. (3). (d) and (e) plot some typical twins equivalence classes (red solid lines) and true twins equivalence classes (blue dashed lines), respectively.

to any other vertex and $\bar{U} = V - U$. An N -qubit graph state $|G_N\rangle$ is defined to be the common $+1$ eigenstate of N vertex stabilizers $\mathcal{S}_i = X_i Z_{\mathcal{A}_i}$ where $Z_{\mathcal{A}_i} \equiv \prod_{j \in \mathcal{A}_i} Z_j$ and $\{X_i, Y_i, Z_i\}$ are the Pauli operators on the i -th qubit [37]. For each nonempty subset of vertices $\alpha \subseteq V$, we have a stabilizer $\mathcal{S}_\alpha = \prod_{i \in \alpha} \mathcal{S}_i \propto X_{S_1} I_{S_2} Y_{S_3} Z_{S_4}$ and correspondingly an optimal local protocol that maximizes the QFI among all choices satisfying the Theorem.

Protocol 1 *For each graph state $|G\rangle$ and a nonempty subset $\alpha \subset V$, the unitary phase estimation model $\rho_\theta = e^{-i\frac{\theta}{2}H_\alpha} |G_N\rangle\langle G_N| e^{i\frac{\theta}{2}H_\alpha}$ with Hamiltonian*

$$H_\alpha = \sum_{j \in (S_1 + S_3) \cap R} Z_j + \sum_{j \in S_1 \cap \bar{R} + S_4 \cap \bar{U}} Y_j + \sum_{j \in S_3 \cap \bar{R} + S_4 \cap U} X_j \quad (1)$$

admits a local protocol with local measurements specified by the stabilizer $\mathcal{S}_\alpha \propto X_{S_1} Y_{S_3} Z_{S_4}$ and corresponding QFI determined by the graph structure

$$\mathcal{F}_\alpha(G) = |\mathcal{S}_\alpha| + 2|T_{S_3 + S_4}| + 2|T_{S_1 + S_4}^*| + 2|L \cap (S_3 + S_4)|, \quad (2)$$

where $|T_\beta| = \sum_m \binom{|\mathcal{V}_m \cap \beta|}{2}$ and $|T_\beta^*| = \sum_m \binom{|\mathcal{U}_m \cap \beta|}{2}$ count the number of pairs of twins and true twins in a subset $\beta \subset V$, respectively.

Some remarks are in order. First, as an example, we consider the ten-qubit graph state in Fig. 1(a) for which $R = \{C, I\}$, $L = \{A, B, D, J\}$, and $\bar{U} = \{F, G\}$. By choosing subset $\alpha = \{C, F, I, J\}$ with corresponding stabilizer $\mathcal{S}_\alpha = X_{\{C, F\}} Y_{\{I, J\}} Z_{\{A, B, D, G\}}$, a local protocol generated by the Hamiltonian $H = X_A + X_B + X_D + X_J + Y_F + Y_G + Z_C + Z_I$ yields a QFI as high as $\mathcal{F}_\alpha(G) = 24$ by local X -measurement on qubits $\{C, F\}$, Y -measurement on qubits $\{I, J\}$, and Z -measurement on qubits $\{A, B, D, G\}$. Second, we can explicitly show that QFI $\mathcal{F}_\alpha(G)$ is an invariant under local Clifford transformation (see the Supplemental Material). According to Theorem, if the unitary

estimation model ($|G_N\rangle\langle G_N|, H, \Omega_V(\theta)$) is a local protocol, so is ($|G_N\rangle\langle G_N|, \tilde{U}H\tilde{U}^\dagger, \tilde{U}\Omega_V(\theta)\tilde{U}^\dagger$), where $|G_N\rangle = \tilde{U}|G_N\rangle$ with $\tilde{U} = \bigotimes_{i \in V} \tilde{U}_i$. This demonstrates that our scheme is invariant under local unitary transformations and necessarily invariant under local Clifford transformations [43, 44]. Thus, Eq. (2) not only identifies the structural features affecting metrological precision but also reveals a certain symmetry of graph states under LU transformations. This provides another perspective for understanding graph states and their equivalence classes [45, 46]. Third, we can upper-bound the optimal QFI Eq. (2) quadratically as

$$\mathcal{F}_\alpha(G) \leq N + 2 \sum_m \binom{|\mathcal{V}_m|}{2} + 2 \sum_m \binom{|\mathcal{U}_m|}{2} + 2|L| := \mathcal{F}(G), \quad (3)$$

which is achievable if and only if there exists a stabilizer $S_a \propto X_{S_1} Y_{S_3} Z_{S_4}$ such that $S_2 = \emptyset$, all true twins in the graph are in $S_1 + S_4$, all twins and all leaf vertices are in $S_3 + S_4$. From the perspective of fewer qubits, the bound Eq. (3) is tight for most graph states; however, there are exceptions, such as the one shown in Fig. 1(c).

Although the upper bound Eq. (3) of QFI is not always tight, it is crucial for estimating the scaling of QFI with N . The QFI upper bound depends on the number of twins or true twins in G_N , and the more equivalence classes of twins (or true twins) and their cardinality, the higher the QFI upper bound. See Figs. 1(d) and (e) for a more intuitive visualization. Also, notably, the QFI can reach the HL if and only if there are approximately $\sim N$ vertices that are mutually twins or mutually true twins. With the above preparation, we now introduce a technique called “subgraph concatenation” to construct as many high-precision scaling graph states as possible. “Subgraph concatenation” treats multiple subgraphs as “vertices”, where the “edges” between these “vertices” correspond to a specific connection between the subgraphs. The structure formed by these “vertices” and “edges” is referred to as a “graph”. Together, the internal structure of the subgraphs and the “graph” form the desired graph we aim to construct.

The first type of state we construct, referred to as A-Type graph states, can choose subgraph s_1 , which contains a single large true twins equivalence class but does not include any twins; subgraph s_2 , which contains a single large twins equivalence class with $|\mathcal{A}_i| = 1$ and its common neighborhood but does not include any true twins; and subgraph s_3 , which contains a large twins equivalence class with $|\mathcal{A}_i| \geq 2$ and its neighborhood but does not include any true twins. The presence of an “edge” between subgraphs $g_1^{(A)}$ and $g_2^{(A)}$ implies that only a very small number of vertices in $g_1^{(A)}$ are connected to a very small number of vertices in $g_2^{(A)}$. The only requirement for the distribution of “edges” between “vertices” in A-Type graph states is to ensure overall connectivity of the graph. The second type of state, B-Type graph states, the presence of an “edge” between subgraphs $g_1^{(B)}$ and $g_2^{(B)}$ implies that any vertex in $g_1^{(B)}$ is connected to all vertices in $g_2^{(B)}$. To obtain B-Type graph states, one first determines a “graph”, ensuring connectivity. Here, the subgraph labelled by s_4 consists only of a set of isolated vertices that are not connected to each other. Then,

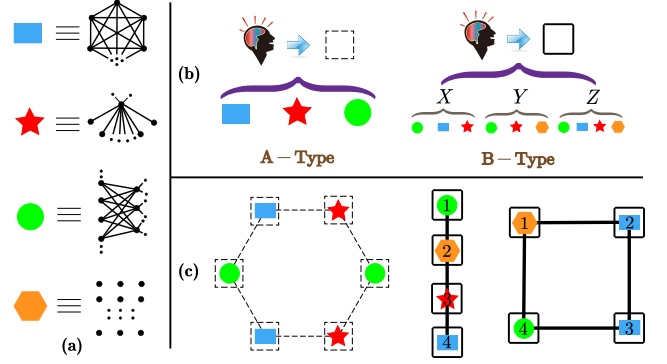


FIG. 2. Construction of A-Type and B-Type graph states. (a) Subgraphs s_1, s_2, s_3 , and s_4 are labelled by blue rectangles, red pentagons, green circles, and orange hexagons, respectively. (b) A-Type subgraphs (dashed squares) can be freely selected from s_1, s_2 and s_3 , as long as the full graph remains connected, regardless of how subgraphs are interconnected. In contrast, the placement of B-Type subgraphs (solid squares) is constrained by the local stabilizer operators: for example, if an X appears at a given position, s_1 may be selected, while a Y would prohibit it. (c) Representative examples of graph structures: from left to right: an A-Type six-subgraph cycle graph, a B-Type four-subgraph cluster graph, and a B-Type four-subgraph cycle graph. For B-Type four-subgraph cluster and cycle graph states the stabilizers used are $X_1 Z_2 Z_3 X_4$ and $Y_1 Z_2 Z_3 Y_4$, respectively.

one provides all full-rank “stabilizers” for this “graph”. Depending on whether the “stabilizer” in each “vertex” position is X, Y , or Z , the subgraphs are filled in at each “vertex” position according to the rules indicated in Fig. 2(b). Each full-rank stabilizer offers a strategy for choosing subgraphs at each position. The above construction and some typical graphs are plotted in Fig. 2.

For two classes of graph states $|G_N^{(A)}\rangle$ and $|G_N^{(B)}\rangle$ there exist stabilizers $S_{\alpha_{A/B}}$ such that $\mathcal{F}_{\alpha_{A/B}}(G^{(A/B)}) \sim \mathcal{F}(G^{(A/B)}) \sim N^{\beta_{A/B}}$, where $\beta_{A/B} > 1$. This indicates that the QFI upper bounds Eq. (3) determined by the structure of the underlying graphs $G^{(A/B)}$ is strictly attainable with scaling in N . For A-Type graph states, the weak correlations between subgraphs lead to the QFI upper bound being approximately the sum of contributions from each subgraph, $\mathcal{F}(G^{(A)}) \sim \sum_{i=1}^{n^{(A)}} (m_i^{(A)})^2$, while for B-Type graph states, the correlations of the structure of the “graph” may further enhance precision, with $\mathcal{F}(G^{(B)}) \gtrsim \sum_{i=1}^{n^{(B)}} (m_i^{(B)})^2$. Here, $n^{(A/B)}$ is the total number of subgraphs and $m_i^{(A/B)}$ is the size of the i -th subgraph in the A/B-Type graph states. Consider a A-type $n^{(A)}$ -subgraph cluster graph state, where $n^{(A)} \sim N^{\frac{1}{3}}, m_1^{(A)} \sim \dots \sim m_{n^{(A)}}^{(A)} \sim N^{\frac{2}{3}}$. We obtain $\mathcal{F} \sim \mathcal{F}_\alpha \sim N^{\frac{5}{3}}$. B-type graph states include the bundled graph states from [12].

Robust Subspace with Invariant Precision Scaling.— Noise is ubiquitous and generally detrimental across quantum technologies. A central goal in noisy quantum metrology is to develop strategies that mitigate noise while preserving precision [47, 48]. Building on our Theorem, we identify a class of high-precision pure-state estimation models that admit local

implementation via Protocol 1. To retain this precision advantage while enhancing noise resilience, we now introduce our second local protocol tailored for mixed states.

Protocol 2 Consider a system of N qubits partitioned into $m+1$ parts, namely, $V = K_1 \sqcup K_2 \sqcup \dots \sqcup K_{m+1}$ with each part containing two or more qubits $|K_\omega| \geq 2$ for $1 \leq \omega \leq m+1$. The unitary phase estimation model $\rho_K(\theta) = e^{-i\frac{\theta}{2}H} \rho_K e^{i\frac{\theta}{2}H}$ with Hamiltonian $H = \sum_j X_j$ and an arbitrary probe state ρ_K living in the 2^m -dimensional subspace \mathcal{P}_K stabilized by

$$\{Z_V\} \cup \{X_{i|\omega} X_{j|\omega} \mid 2 \leq j \leq |K_\omega|; 1 \leq \omega \leq m+1\} \quad (4)$$

where the subscript $i|\omega$ denotes the i -th qubit in K_ω , admits a local protocol with local measurements being $e^{-i\frac{\theta}{2}X_j} Z_j e^{i\frac{\theta}{2}X_j}$ for all qubits achieving the corresponding QFI

$$\mathcal{F}[\rho_K(\theta)] = \sum_{\lambda \in \mathbb{F}_2^m} \langle d_\lambda | \rho_K | d_\lambda \rangle \left(N - 2 \sum_{\omega \geq 2} \lambda_{\omega-1} |K_\omega| \right)^2, \quad (5)$$

where $\{|d_\lambda\rangle = \prod_{\omega \geq 2} Z_{K_\omega}^{\lambda_{\omega-1}} |\text{GHZ}_N\rangle\}_{\lambda \in \mathbb{F}_2^m}$ spans \mathcal{P}_K .

With the fixed subspace \mathcal{P}_K , the QFI $\mathcal{F}[\rho_K(\theta)]$ reaches its maximum $\max_{\rho_K} \mathcal{F}[\rho_K(\theta)] = N^2$ at GHZ state and its minimum is given by $\min_{\rho_K} \mathcal{F}[\rho_K(\theta)] = N^2 r_{K,\min}$, where $r_{K,\min} \equiv \min_{\lambda} [1 - 2 \sum_{\omega \geq 2} \lambda_{\omega-1} \xi_\omega]^2$ depends on the relative magnitudes of $\xi_\omega = \frac{|K_\omega|}{N}$. All values in between are possible. It can be seen that as long as $r_{K,\min} \gtrsim N^{-\epsilon}$, we have $N^{2-\epsilon} \leq \mathcal{F}[\rho_K(\theta)] \leq N^2$. Thus, the subspace can be regarded as a probe state subspace with approximately scale-invariant precision within the interval $[2 - \epsilon, 2]$, where ϵ is referred to as the tolerance, indicating the allowed degree of scaling deviation compared to the HL. As $\epsilon \rightarrow 0^+$, the subspace becomes a strictly HL scale-invariant subspace. It is apparent that one can construct sufficiently many \mathcal{P}_K to meet the above requirements, including but not limited to the following three types of situations: (i) there exists $\omega \in \{1, 2, \dots, m+1\}$ such that $\frac{1+\delta_1}{2} < \xi_\omega < 1$, where $0 < \delta_1 < 1$, which implies that the tolerance $\epsilon < -\frac{2 \log \delta_1}{\log N}$; (ii) $2 \leq m \sim N^{\delta_2}$ and m is even, $\xi_1 = \xi_2 = \dots = \xi_{m+1} = \frac{N}{m+1}$, which leads to the tolerance $\epsilon \sim \frac{2\delta_2}{\log N}$; (iii) $m \sim N^{\delta_3}$ and m is odd, $\xi_1 \ll \frac{1}{2m}$, $\xi_2 = \frac{1}{m} - \xi_1$, and if $m \geq 3$, $\xi_3 = \dots = \xi_{m+1} = \frac{N}{m}$, which gives the tolerance $\epsilon \sim \frac{2\delta_3}{\log N}$.

Define $\mathbb{P}_\epsilon \equiv \{\mathcal{P}_K \mid N^{2-\epsilon} \leq \mathcal{F}[\rho_K(\theta)] \leq N^2\}$ as the set of subspaces with ϵ -tolerance corresponding to different partitions K . We declare \mathbb{P}_ϵ as a subspace of probe states with “full metrological advantages”, featuring local protocols, near-scale-invariant high precision, partial noise resistance, and full noise correction. Beyond providing more usable resource states, \mathbb{P}_ϵ offers a quantitative framework to understand the precision-robustness trade-off and allows on-demand control.

Select ρ_{K_1} from the subspace $\mathcal{P}_{K_1} \in \mathbb{P}_\epsilon$ as the probe state. For any $\mathcal{P}_{K_2} \in \mathbb{P}_\epsilon$, noise \mathcal{D}_1 satisfying $\mathcal{D}_1(\rho_{K_1}) = \rho_{K_2} \in \mathcal{P}_{K_2}$ is robust for ρ_{K_1} within the precision scaling tolerance interval $[2 - \epsilon, 2]$, provided \mathcal{D}_1 occurs before parameter encoding, after parameter encoding with $\theta \approx 0$, or commutes with the evolution Hamiltonian H' , regardless of its form or

source. Furthermore, if quantum error correction (QEC) is allowed before parameter encoding. Then irrespective of the type of noise \mathcal{D}_2 affecting the state prior to parameter encoding (e.g., during the preparation of the probe state), as long as for $\forall \omega \in \{1, \dots, m+1\}$, $|K_\omega| > \Upsilon_e$ holds, we can always construct a QEC scheme \mathcal{E} involving only local measurements and local recovery operations, such that the corrected probe state $\rho_{\text{corr}} \equiv \mathcal{E}[\mathcal{D}_2(\rho_K)]$ retains the same QFI as ρ_K , that is

$$\mathcal{F}[e^{-i\frac{\theta}{2}H'} \rho_{\text{corr}} e^{i\frac{\theta}{2}H'}] = \mathcal{F}[e^{-i\frac{\theta}{2}H'} \rho_K e^{i\frac{\theta}{2}H'}]. \quad (6)$$

Here, $\Upsilon_e \in \mathbb{Z}^+$ depends on e in e -qubit errors. \mathcal{E} is not a traditional quantum error correction scheme, as it does not require $\rho_{\text{corr}} = \rho_K$ (it is nearly impossible to achieve), the consistency of the QFI is sufficient to meet our goals [27].

Behavior Under Dephasing Noise.—The GHZ state $|\text{GHZ}_N\rangle = \frac{1}{\sqrt{2}}(|+\rangle^{\otimes N} + |-\rangle^{\otimes N})$ as a widely studied multi-qubit entangled probe state in quantum metrology performs exceptionally well in ideal environments. However, the rapid decay of QFI under various types of noise - especially dephasing - significantly limits its practical applicability. Assume that an N -qubit probe state ρ is subjected to i.i.d. dephasing noise during parameter encoding, the encoded state is thus given by $\tilde{\rho}_\theta = \left(\bigotimes_{j \in V} \mathcal{L}_\theta^{(j)}\right)(\rho)$, where $\mathcal{L}_\theta^{(j)}(\rho) \equiv p X_j e^{-i\frac{\theta}{2}X_j} \rho e^{i\frac{\theta}{2}X_j} X_j + (1-p) e^{-i\frac{\theta}{2}X_j} \rho e^{i\frac{\theta}{2}X_j}$ acts on the j -th qubit, and $0 < p < \frac{1}{2}$ is the dephasing probability. When $\rho = |\text{GHZ}_N\rangle\langle\text{GHZ}_N|$, one can show that the QFI $\mathcal{F}_{\text{dap}}(p, \rho) \equiv \mathcal{F}(\tilde{\rho}_\theta) = N^2(1-2p)^{2N}$ decays exponentially with the increase of N . When choosing $\rho = \rho_K \in \mathcal{P}_K$, as long as ρ_K tends to be distributed within the interior of \mathcal{P}_K , it will exhibit greater resistance to dephasing noise compared to the GHZ state. To observe this, as shown in Fig. 3(a), although $|\text{GHZ}_N\rangle\langle\text{GHZ}_N|$ shows a notable precision advantage at $p \approx 0$, as p increases, the decay trend of the QFI for ρ_K , whether pure or mixed and for any value of m , is

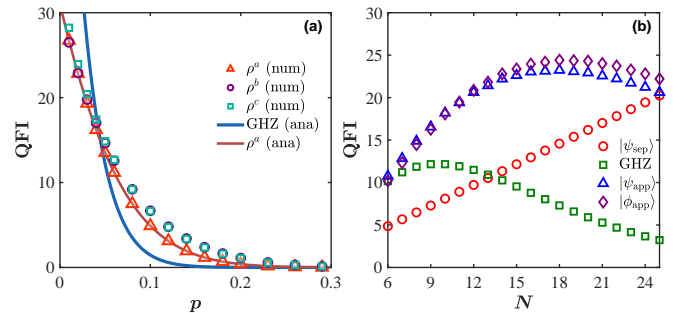


FIG. 3. Robustness advantage of ρ_K compared to the GHZ state under i.i.d. dephasing noise ($\theta = 0.3$). (a) $\mathcal{F}_{\text{dap}}(p, \rho)$ as a function of dephasing probability p , evaluated for four probe states: a pure state $\rho^a \in \mathcal{P}_{(4,5)}$, a pure state $\rho^b \in \mathcal{P}_{(3,3,3)}$, a mixed state $\rho^c \in \mathcal{P}_{(3,3,3)}$, and the GHZ state $|\text{GHZ}_N\rangle$, with fixed system size $N = 9$. “Ana” and “num” denote analytical and numerical results, respectively. (b) $\mathcal{F}_{\text{dap}}(p, \rho)$ versus the size N of the system for fixed dephasing probability $p = 0.05$. The pure state $|\psi_{\text{app}}\rangle$ and $|\phi_{\text{app}}\rangle$ selected from $\mathcal{P}_{\lfloor \frac{N}{2} \rfloor, N - \lfloor \frac{N}{2} \rfloor}$ are compared with the GHZ state $|\text{GHZ}_N\rangle$ and the fully separable state $|\psi_{\text{sep}}\rangle = |0\rangle^{\otimes N}$. Detailed expressions of $|\psi_{\text{app}}\rangle$ and $|\phi_{\text{app}}\rangle$ can be found in the SM.

slower than that of the GHZ state.

To further the robustness to noise of the subspace \mathcal{P}_K , two appropriately selected pure states $|\psi_{\text{app}}\rangle$ and $|\phi_{\text{app}}\rangle$ from $\mathcal{P}_{\lfloor \frac{N}{2} \rfloor, N - \lfloor \frac{N}{2} \rfloor}$ are compared with the GHZ state $|\text{GHZ}_N\rangle$. The QFIs show a qualitative difference in its scaling with N , as illustrated in Fig. 3(b). Moreover, even when compared to the most noise-resilient fully separable state $|\psi_{\text{sep}}\rangle$, the advantage persists even for system sizes up to $N \lesssim 25$ when $p = 0.05$, which is significantly larger than the GHZ state's threshold of $N \lesssim 14$.

Conclusion.— In this work, by constructing sufficient criteria for local measurements to satisfy the QCRB and developing optimal parameter estimation schemes for both noiseless and noisy environments, we have identified a series of multi-qubit probe states that achieve high precision through local measurements while maintaining noise resistance. We found that stabilizers are a broad class of quantum resources within the more experimentally feasible framework of local measurement-based quantum metrology. Their significance

lies not only in enhancing measurement precision but also in providing reference templates for optimal local measurements and balancing noise robustness. We anticipate the near-term application of our theoretical schemes to physical platforms such as Rydberg atoms [49–51]. Future research directions include extending our theory to high-dimensional quantum systems (qudits) [52] and continuous-variable systems [53, 54], among others.

Acknowledgments. — We thank Jing Yang and Weizhe Gao for helpful discussions. HLS was supported by the European Commission through the H2020 QuantERA ERANET Cofund in Quantum Technologies project “MENTA” and the NSFC key grants No. 12134015 and No. 92365202. CW is supported by the National Research Foundation, Singapore and A*STAR under its Quantum Engineering Programme (NRF2021-QEP2-02-P03). SY was supported by Innovation Program for Quantum Science and Technology (2021ZD0300804).

-
- [1] C. M. Caves, Quantum-mechanical noise in an interferometer, *Phys. Rev. D* **23**, 1693 (1981).
 - [2] V. Giovannetti, S. Lloyd, and L. Maccone, Quantum-Enhanced Measurements: Beating the Standard Quantum Limit, *Science* **306**, 1330 (2004).
 - [3] V. Giovannetti, S. Lloyd, and L. Maccone, Advances in quantum metrology, *Nat. Photonics* **5**, 222 (2011).
 - [4] G. Tóth and I. Apellaniz, Quantum metrology from a quantum information science perspective, *J. Phys. A* **47**, 424006 (2014).
 - [5] L. Pezzè, A. Smerzi, M. K. Oberthaler, R. Schmied, and P. Treutlein, Quantum metrology with nonclassical states of atomic ensembles, *Rev. Mod. Phys.* **90**, 035005 (2018).
 - [6] C. L. Degen, F. Reinhard, and P. Cappellaro, Quantum sensing, *Rev. Mod. Phys.* **89**, 035002 (2017).
 - [7] S. Zhou, C.-L. Zou, and L. Jiang, Saturating the quantum Cramér-Rao bound using LOCC, *Quantum Sci. Technol.* **5**, 025005 (2020).
 - [8] S. Boixo, A. Datta, S. T. Flammia, A. Shaji, E. Bagan, and C. M. Caves, Quantum-limited metrology with product states, *Phys. Rev. A* **77**, 012317 (2008).
 - [9] S. M. Roy and S. L. Braunstein, Exponentially enhanced quantum metrology, *Phys. Rev. Lett.* **100**, 220501 (2008).
 - [10] M. M. Rams, P. Sierant, O. Dutta, P. Horodecki, and J. Zakrzewski, At the limits of criticality-based quantum metrology: Apparent super-heisenberg scaling revisited, *Phys. Rev. X* **8**, 021022 (2018).
 - [11] J. Joo, W. J. Munro, and T. P. Spiller, Quantum Metrology with Entangled Coherent States, *Phys. Rev. Lett.* **107**, 083601 (2011).
 - [12] N. Shettell and D. Markham, Graph States as a Resource for Quantum Metrology, *Phys. Rev. Lett.* **124**, 110502 (2020).
 - [13] Y. Yang, B. Yadin, and Z.-P. Xu, Quantum-Enhanced Metrology with Network States, *Phys. Rev. Lett.* **132**, 210801 (2024).
 - [14] D. M. Greenberger, M. A. Horne, A. Shimony, and A. Zeilinger, Bell's theorem without inequalities, *Am. J. Phys.* **58**, 1131 (1990).
 - [15] V. Giovannetti, S. Lloyd, and L. Maccone, Quantum Metrology, *Phys. Rev. Lett.* **96**, 010401 (2006).
 - [16] A. Streltsov, G. Adesso, and M. B. Plenio, Colloquium: Quantum coherence as a resource, *Rev. Mod. Phys.* **89**, 041003 (2017).
 - [17] C. Zhang, T. R. Bromley, Y.-F. Huang, H. Cao, W.-M. Lv, B.-H. Liu, C.-F. Li, G.-C. Guo, M. Cianciaruso, and G. Adesso, Demonstrating quantum coherence and metrology that is resilient to transversal noise, *Phys. Rev. Lett.* **123**, 180504 (2019).
 - [18] A. Castellini, R. Lo Franco, L. Lami, A. Winter, G. Adesso, and G. Compagno, Indistinguishability-enabled coherence for quantum metrology, *Phys. Rev. A* **100**, 012308 (2019).
 - [19] S. F. Huelga, C. Macchiavello, T. Pellizzari, A. K. Ekert, M. B. Plenio, and J. I. Cirac, Improvement of frequency standards with quantum entanglement, *Phys. Rev. Lett.* **79**, 3865 (1997).
 - [20] B. M. Escher, R. L. de Matos Filho, and L. Davidovich, General framework for estimating the ultimate precision limit in noisy quantum-enhanced metrology, *Nat. Phys.* **7**, 406 (2011).
 - [21] R. Demkowicz-Dobrzański, J. Kołodyński, and M. Guţă, The elusive heisenberg limit in quantum-enhanced metrology, *Nat. Commun.* **3**, 1063 (2012).
 - [22] R. Demkowicz-Dobrzański and L. Maccone, Using entanglement against noise in quantum metrology, *Phys. Rev. Lett.* **113**, 250801 (2014).
 - [23] J. Preskill, Quantum Computing in the NISQ era and beyond, *Quantum* **2**, 79 (2018).
 - [24] K. Bharti, A. Cervera-Lierta, T. H. Kyaw, T. Haug, S. Alperin-Lea, A. Anand, M. Degroote, H. Heimonen, J. S. Kottmann, T. Menke, W.-K. Mok, S. Sim, L.-C. Kwek, and A. Aspuru-Guzik, Noisy intermediate-scale quantum algorithms, *Rev. Mod. Phys.* **94**, 015004 (2022).
 - [25] W. Dür, M. Skotiniotis, F. Fröwis, and B. Kraus, Improved quantum metrology using quantum error correction, *Phys. Rev. Lett.* **112**, 080801 (2014).
 - [26] E. M. Kessler, I. Lovchinsky, A. O. Sushkov, and M. D. Lukin, Quantum error correction for metrology, *Phys. Rev. Lett.* **112**, 150802 (2014).
 - [27] X.-M. Lu, S. Yu, and C. H. Oh, Robust quantum metrological schemes based on protection of quantum fisher information, *Nat. Commun.* **6**, 7282 (2015).
 - [28] S. Zhou, M. Zhang, J. Preskill, and L. Jiang, Achieving the Heisenberg limit in quantum metrology using quantum error

- correction, *Nat. Commun.* **9**, 78 (2018).
- [29] J. M. Taylor, P. Cappellaro, L. Childress, L. Jiang, D. Budker, P. R. Hemmer, A. Yacoby, R. Walsworth, and M. D. Lukin, High-sensitivity diamond magnetometer with nanoscale resolution, *Nat. Phys.* **4**, 810 (2008).
 - [30] P. Sekatski, M. Skotiniotis, and W. Dür, Dynamical decoupling leads to improved scaling in noisy quantum metrology, *New J. Phys.* **18**, 073034 (2016).
 - [31] L. M. Pham, N. Bar-Gill, C. Belthangady, D. Le Sage, P. Cappellaro, M. D. Lukin, A. Yacoby, and R. L. Walsworth, Enhanced solid-state multispin metrology using dynamical decoupling, *Phys. Rev. B* **86**, 045214 (2012).
 - [32] A. W. Chin, S. F. Huelga, and M. B. Plenio, Quantum metrology in non-markovian environments, *Phys. Rev. Lett.* **109**, 233601 (2012).
 - [33] Z. H. Saleem, A. Shaji, and S. K. Gray, Optimal time for sensing in open quantum systems, *Phys. Rev. A* **108**, 022413 (2023).
 - [34] M. Hirose and P. Cappellaro, Coherent feedback control of a single qubit in diamond, *Nature* **532**, 77 (2016).
 - [35] Q. Zheng, L. Ge, Y. Yao, and Q.-j. Zhi, Enhancing parameter precision of optimal quantum estimation by direct quantum feedback, *Phys. Rev. A* **91**, 033805 (2015).
 - [36] J. Liu and H. Yuan, Quantum parameter estimation with optimal control, *Phys. Rev. A* **96**, 012117 (2017).
 - [37] M. Hein, J. Eisert, and H. J. Briegel, Multiparty entanglement in graph states, *Phys. Rev. A* **69**, 062311 (2004).
 - [38] J. Liu, H. Yuan, X.-M. Lu, and X. Wang, Quantum fisher information matrix and multiparameter estimation, *J. Phys. A: Math. Theor.* **53**, 023001 (2019).
 - [39] C. W. Helstrom, Quantum detection and estimation theory, *J. Stat. Phys.* **1**, 231 (1969).
 - [40] S. L. Braunstein and C. M. Caves, Statistical distance and the geometry of quantum states, *Phys. Rev. Lett.* **72**, 3439 (1994).
 - [41] N. Friis, D. Orsucci, M. Skotiniotis, P. Sekatski, V. Dunjko, H. J. Briegel, and W. Dür, Flexible resources for quantum metrology, *New J. Phys.* **19**, 063044 (2017).
 - [42] J.-X. Liu, J. Yang, H.-L. Shi, and S. Yu, Optimal local measurements in single-parameter quantum metrology, *Phys. Rev. A* **111**, 022436 (2025).
 - [43] M. Van den Nest, J. Dehaene, and B. De Moor, Local unitary versus local clifford equivalence of stabilizer states, *Phys. Rev. A* **71**, 062323 (2005).
 - [44] B. Zeng, H. Chung, A. W. Cross, and I. L. Chuang, Local unitary versus local clifford equivalence of stabilizer and graph states, *Phys. Rev. A* **75**, 032325 (2007).
 - [45] A. Cabello, L. E. Danielsen, A. J. López-Tarrida, and J. R. Portillo, Optimal preparation of graph states, *Phys. Rev. A* **83**, 042314 (2011).
 - [46] L. Vandr , J. de Jong, F. Hahn, A. Burchardt, O. G hne, and A. Pappa, Distinguishing graph states by the properties of their marginals, [arXiv:2406.09956](https://arxiv.org/abs/2406.09956) [quant-ph].
 - [47] D. Layden and P. Cappellaro, Spatial noise filtering through error correction for quantum sensing, *npj Quantum Inf* **4**, 30 (2018).
 - [48] S. Zhou and L. Jiang, Optimal approximate quantum error correction for quantum metrology, *Phys. Rev. Res.* **2**, 013235 (2020).
 - [49] D.-S. Ding, Z.-K. Liu, B.-S. Shi, G.-C. Guo, K. M lmer, and C. S. Adams, Enhanced metrology at the critical point of a many-body Rydberg atomic system, *Nat. Phys.* **18**, 1447 (2022).
 - [50] M. Saffman, T. G. Walker, and K. M lmer, Quantum information with rydberg atoms, *Rev. Mod. Phys.* **82**, 2313 (2010).
 - [51] Z. Qin and V. W. Scarola, Scaling of computational order parameters in Rydberg atom graph states, [arXiv:2409.05941](https://arxiv.org/abs/2409.05941) [quant-ph].
 - [52] Y. Wang, Z. Hu, B. C. Sanders, and S. Kais, Qudits and High-Dimensional Quantum Computing, *Front. Phys.* **8** (2020).
 - [53] Y. Wang and K. Fang, Continuous-variable graph states for quantum metrology, *Phys. Rev. A* **102**, 052601 (2020).
 - [54] H. Kwon, Y. Lim, L. Jiang, H. Jeong, and C. Oh, Quantum Metrological Power of Continuous-Variable Quantum Networks, *Phys. Rev. Lett.* **128**, 180503 (2022).